



# Modal Characterization using Principal Component Analysis: application to Bessel, higher-order Gaussian beams and their superposition

A. Mourka<sup>1</sup>, M. Mazilu<sup>1</sup>, E. M. Wright<sup>1,2</sup> & K. Dholakia<sup>1,2</sup>

<sup>1</sup>SUPA, School of Physics and Astronomy, University of St. Andrews, North Haugh, St. Andrews KY16 9SS, UK, <sup>2</sup>College of Optical Sciences, The University of Arizona, 1630 East University Boulevard, Tuscon, Arizona 85721-0094, USA.

SUBJECT AREAS:  
OPTICS AND PHOTONICS  
PHYSICS  
ADAPTIVE OPTICS  
APPLIED PHYSICS

Received  
25 September 2012

Accepted  
26 February 2013

Published  
12 March 2013

Correspondence and  
requests for materials  
should be addressed to  
M.M. (michael.  
mazilu@st-andrews.  
ac.uk)

The modal characterization of various families of beams is a topic of current interest. We recently reported a new method for the simultaneous determination of both the azimuthal and radial mode indices for light fields possessing orbital angular momentum. The method is based upon probing the far-field diffraction pattern from a random aperture and using the recorded data as a ‘training set’. We then transform the observed data into uncorrelated variables using the principal component analysis (PCA) algorithm. Here, we show the generic nature of this approach for the simultaneous determination of the modal parameters of Hermite-Gaussian and Bessel beams. This reinforces the widespread applicability of this method for applications including information processing, spectroscopy and manipulation. Additionally, preliminary results demonstrate reliable decomposition of superpositions of Laguerre-Gaussians, yielding the intensities and relative phases of each constituent mode. Thus, this approach represents a powerful method for characterizing the optical multi-dimensional Hilbert space.

The characterization of the modal decomposition of light remains a key requirement in numerous fields in optics. This includes classical and quantum information processing<sup>1</sup>, laser resonator dynamics<sup>2</sup>, fiber optics delivery of light<sup>3–5</sup> and the orbital angular momentum of light<sup>6,7</sup>. A number of schemes for characterizing such fields have emerged that rely upon exploration of the far-field diffraction pattern of the field but pure inspection of the form of the pattern is insufficient to delineate the desired modal parameters in a robust manner. Identification of (for example) Laguerre-Gaussian (LG) beams has been recently shown using diffractive structures such as arrays of pinholes<sup>8</sup> and a triangular aperture<sup>9,10</sup>. Furthermore, researchers have also used slits<sup>11,12</sup>, and holograms<sup>13,14</sup>. However, all these experimentally realized approaches can be used to measure only one single degree of freedom (the azimuthal index) of the LG beams, neglecting the radial component and indeed have never been applied to other families of light beams. Furthermore, open questions include the optimal aperture to use and how robust the determination of mode indices is in the presence of any misalignment. Recently, we developed a method using multivariate analysis to obtain both the radial and azimuthal mode indices simultaneously for light fields possessing orbital angular momentum<sup>15</sup>. Our studies are reinforced by theoretical work on the angular and radial mode analysis of optical beams<sup>16</sup> that deals with decomposition of beam into LG components using a Mach Zehnder scheme. However this method does not measure the relative phase between the modes and it needs multiple exposures.

Our PCA approach is based on ‘training’ our optical system with the measured far-field diffraction patterns from known pure incident light fields upon a random diffuser and transforming the observed patterns into uncorrelated variables using the principal component analysis (PCA) algorithm.

It is important to establish the validity of our method for the other families of light fields to demonstrate its full applicability. In this regard Hermite-Gaussian (HG) modes are of major interest in laser resonator output analysis<sup>17</sup> and spectroscopy<sup>18</sup>. Pure HG modes are characterized by nodes in orthogonal directions in a Cartesian co-ordinate space as is well documented<sup>19</sup>. Bessel light modes offer new directions in manipulation<sup>20</sup>, nanosurgery<sup>21</sup>, microscopy<sup>22</sup> and are delineated again by an azimuthal index  $m$  and a radial  $k$ -vector. Both of these fields are also of interest for information processing<sup>23</sup>.



In this paper, we demonstrate the application of our multivariate analysis approach for modal characterization of both Hermite-Gaussian and Bessel beams. We report the variations between the different far-field diffraction patterns of both HG and Bessel beams from a random aperture (glass diffuser), upon which we perform PCA. The different far-field diffraction patterns contain information for the different mode indices for the considered laser beam modes. Using PCA the optical system is ‘trained’ and it is subsequently possible to simultaneously determine the modal characteristics of ‘unknown’ Hermite-Gaussian or Bessel beams incident upon our random aperture. Additionally, we investigate the role of rotational misalignments upon our method. This further degree of freedom is particularly important when considering Hermite-Gaussian beams, which compared to LG or Bessel beams do not possess a cylindrical symmetry.

In the last part of the paper, we consider the applicability of the PCA method to characterize the complex superposition of LG beams i.e. the detected beams are not pure modes but the result of a general linear superposition of these modes. Here, we generalize the method presented previously<sup>15</sup> by using an optical eigenmode<sup>31,32</sup> decomposition together with a Gerchberg-Saxton (GS) algorithm<sup>33</sup>. We show that our thus extended method is able to measure the complex amplitudes of the different LG components in a limited superposition of LG beams, key for practical applications.

## Results

**Modal characterization of Hermite-Gaussian beams.** To illustrate our generic approach we first begin with a discussion of propagating

Hermite-Gaussian (HG) beams. For each different HG beam mode we considered, we recorded its pattern for 1000 beam samples. The ‘training step’ is firstly applied, in which the response of the optical diffracting system is measured for every HG beam mode, each with different  $m$  and  $n$  values. The beam mode indices  $m$  and  $n$  could vary from 0 to 6, with step equal to 1, yielding seven different values for each. In this manner, a database of all the possible forty-nine HG beams is created. Then the PCA algorithm is used, in order to create the covariance matrix of all the recorded patterns, by subtraction of the common mean intensity of these recorded intensity patterns. The data set is rotated, according to the PCA algorithm, around its centre in order to find the orientation that delivers the largest variation along an axis. This axis corresponds to the first principal component (PC1). In a second step, the PCA algorithm further rotates the data set, leaving PC1 invariant, in order to find a second axis, perpendicular to PC1, showing the second largest variation. This corresponds to the second principal component (PC2). This process can be repeated until all major variance of the dataset are taken into account. The first nine principal components (PCs) of the measure are shown in Figure 1b. The intensity patterns of the ‘unknown’ beam modes can be represented in the same way, using the method of the nearest neighbor measurement in order to classify them<sup>24</sup>. The experimentally observed transverse intensity profiles of the slightly rotated lowest-order HG beams are presented in Figure 1a. The effect of the rotation of the HG beams is studied in a later section. As seen by ‘training’ our optical system by using the first nine PCs, 100% classification efficiency for the detection of the ‘unknown’ propagating HG beams can be achieved. By the same

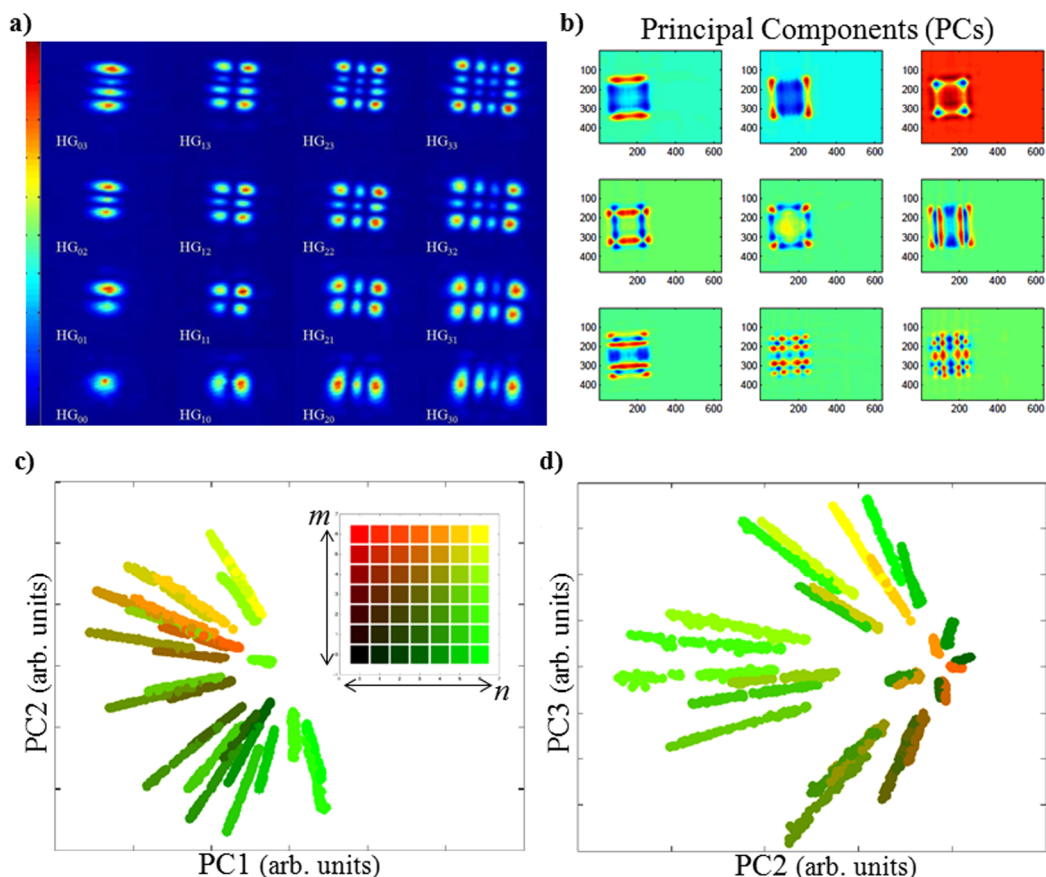


**Figure 1 | Modal characterization of propagating Hermite-Gaussian (HG) beam modes.** (a) The experimentally observed transverse intensity profiles of the lowest-order Hermite-Gaussian beam modes, starting with  $HG_{00}$  (lower left-hand side) and going up to  $HG_{33}$  (upper right-hand side). The color coded for the intensity is highlighted on the left-hand side where the blue and the red colors indicate the lower and higher intensity respectively, (b) the first 9 principal components (PCs) of the measure, (c) first two principal components analysis and color coded for the  $m$  and  $n$  indices of the HG beam modes ( $m = [0, 6]$ ,  $n = [0, 6]$ ), and (d) second and third principal components analysis.

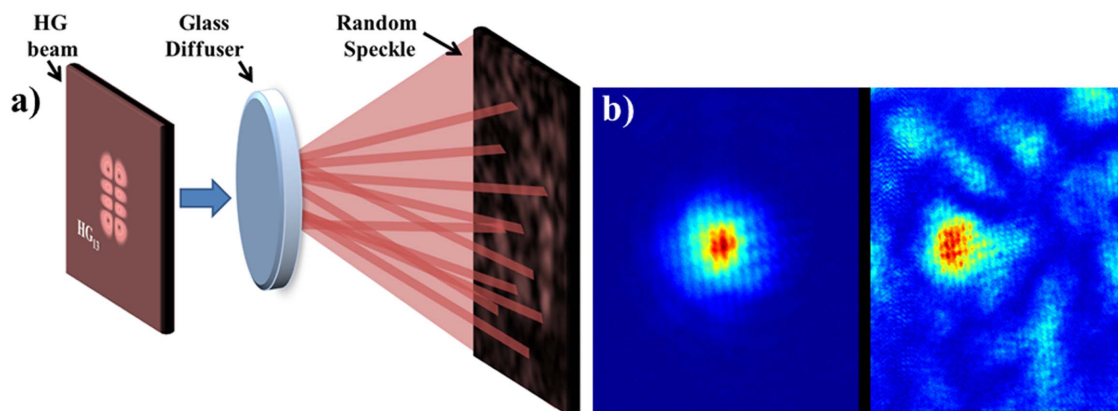


**Figure 2 | Experimental implementation of the random aperture.** (a) Design of the experiment where a HG mode ( $HG_{13}$ ) is focused on a glass diffuser aperture and a speckle pattern is transmitted and (b) (See Supplementary video file S1) the video includes an animation in which the incident  $HG_{00}$  beam mode is presented on the left-hand side while on the right-hand side the resulting speckle pattern from its diffraction from the glass diffuser takes place.

token, all the ‘unknown’ HG beam modes have been correctly identified as the expected HG beam modes.

We then considered the diffraction of Hermite-Gaussian beams from a glass diffuser. This is an aperture that can break the symmetry of a given HG beam mode and, as might be expected speckle patterns result (Figure 2a). Here, the resulting speckle patterns from the diffraction of Hermite-Gaussian beams from a glass diffuser can be used to probe the modal characteristics of the HG beams (Figure 2b). In Figure 3 we see the range of speckle patterns that result from the random perturbation of the glass diffuser and their subsequent analysis. Furthermore, it is to be noted that the use of a random aperture

presents an experimental benefit as all diffraction patterns have similar peak intensities enabling acquisition with similar exposure durations. Remarkably, using this ‘random’ aperture we achieve 100% classification efficiency, by ‘training’ our optical system using the first nine PCs, as indeed for the propagating beams (Figure 3d).

The fundamental question of beam misalignment in the optical system and the impact upon the detection efficiency is also very interesting. We therefore investigated the influence of the beam rotation around its central optical axis, on the classification ability of our method. This can be done by controllably rotating the SLM mask used to generate the considered beams. Here, we studied the effect of

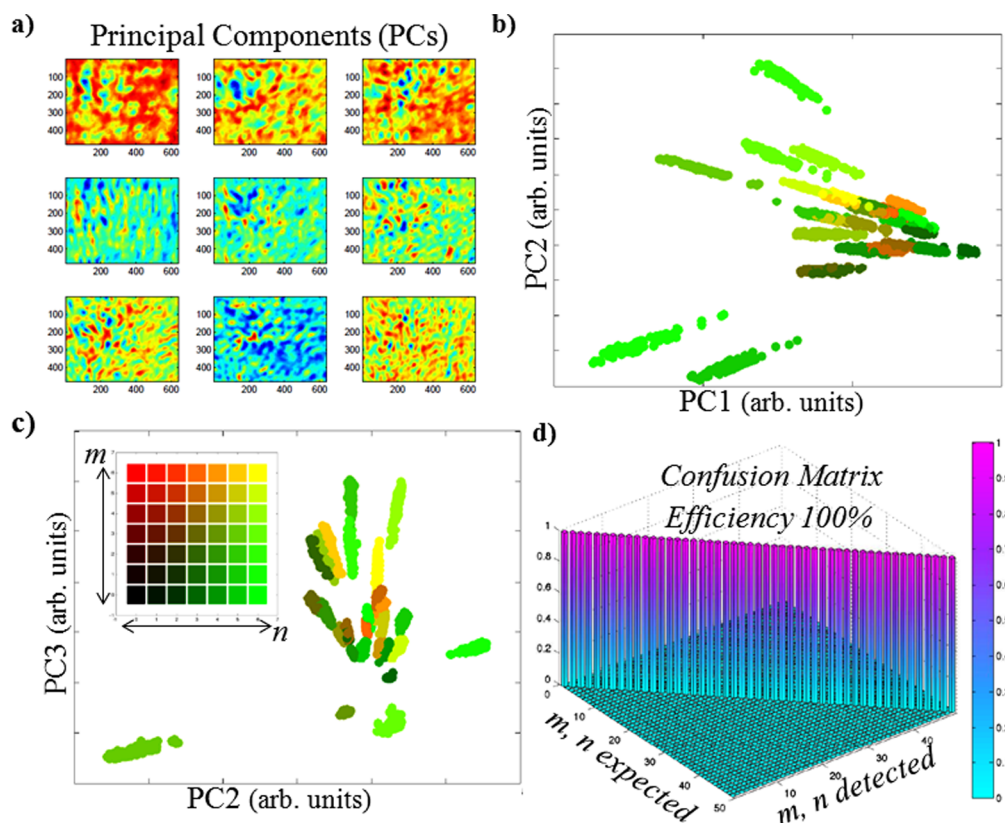


**Figure 3 | Modal characterization of the diffracted Hermite-Gaussian (HG) beams from a random aperture.** (a) The first 9 principal components of the measure, (b) analysis for the first two principal components, (c) analysis for the second and third principal components and color coded for the  $m$  and  $n$  indices of the HG beam modes ( $m = [0, 6]$ ,  $n = [0, 6]$ ), and (d) the 3D chart of the confusion matrix linking the expected and detected indices of the HG beam modes.

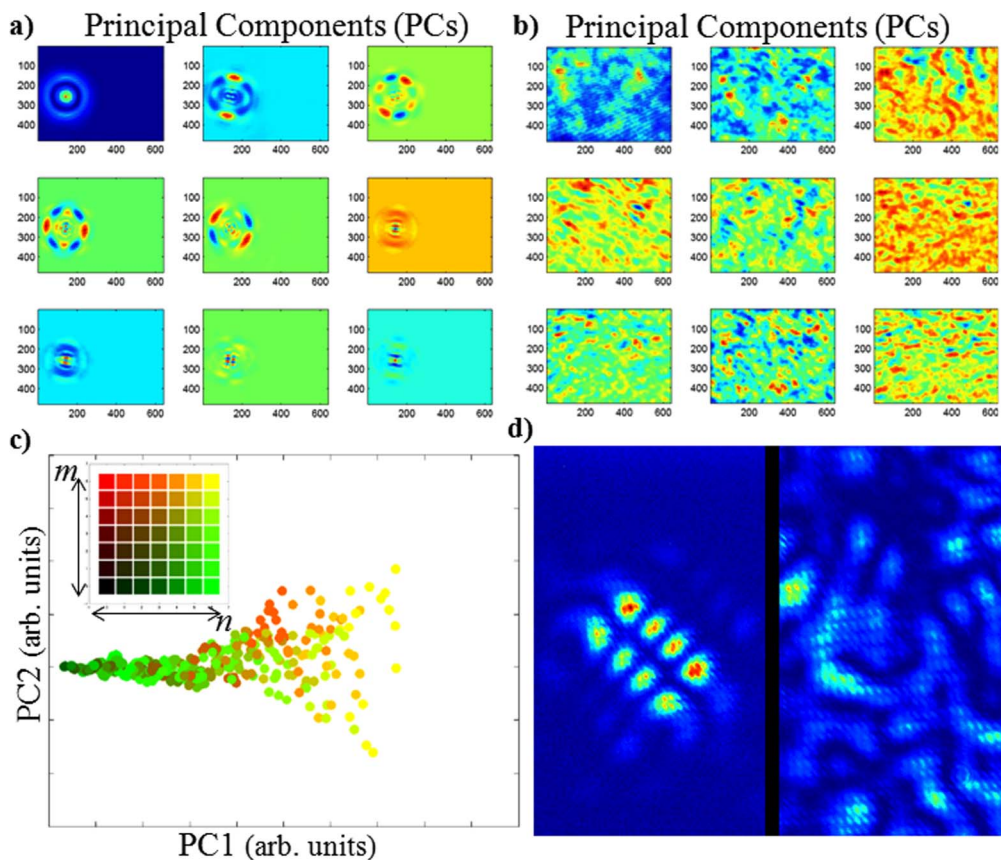


**Figure 4 | Modal characterization of the rotated Hermite-Gaussian (HG) beams which were diffracted from a random aperture.** (a) The first 9 principal components of the rotated HG beam modes, (b) the first 9 principal components of the diffracted HG beam modes from a random aperture and their (c) first and second principal components analysis and color coded for the  $m$  and  $n$  mode indices of the HG beams, and (d) (See Supplementary video file S2) the video includes an animation in which the rotated HG<sub>31</sub> beam mode is presented on the left-hand side while on the right-hand side the resulting speckle pattern from its diffraction from the glass diffuser takes place.

rotation angles from  $-7\pi/32$  to  $7\pi/32$ . The PCA ‘training step’ was done using 15 rotated beams in the studied range. By using the first nine PCs, we observed 99% classification efficiency for correctly identifying the ‘unknown’ HG beam mode even in presence of rotation (Figure 4). This may prove very useful for applications such as beam converters and laser resonators, where the beam alignment is crucial<sup>25–28</sup>. As previously discussed<sup>15</sup>, this detection method can accommodate a certain degree of misalignment or variations in the optical system. Since the correct detection can still be achieved, provided that either a larger ‘training set’ is considered and/or a larger dimensionality of the data is allowed by taking more PCs into account. Our PCA detection method is limited by the number of detectable degrees of freedom of the far-field diffraction patterns<sup>29</sup>. Indeed, low resolution cameras would greatly decrease the distinguishability between the different beams and decrease the number of modes that can be detected in a complex superposition. We also note that very specific misalignments, such as a rotation by  $\pi/2$  for example, would make some HG modes indistinguishable. We can deduce from this statement that the PCA method is also limited by specific beam dependence misalignments. The precise limitation can be assessed by considering the optical degrees of freedom (see section on modal characterization of Laguerre-Gaussian beam superposition).

**Modal characterization of diffracted Bessel beams.** We now apply our PCA detection method to Bessel beams. Forty-nine different Bessel beam modes were considered. We explored beams where the azimuthal index  $m$ , varied from  $-3$  to  $3$  with integer step sizes,

and for seven different values of the radial index  $k_r$ . This maintains the same dimensionality used before for the Hermite-Gaussian beams analysis. The far-field diffraction patterns of the diffracted Bessel beams from a random (glass diffuser) aperture were considered. First the ‘training step’ is applied in which the response of the optical diffracting system is measured for every single Bessel beam considered. Then the second step followed, where we used the classification algorithm which corresponds to the actual identification or measurement of an ‘unknown’ Bessel beam, delivering simultaneously the mode indices which characterize this beam. As depicted in Figure 5, the classification results again displaying 100% efficiency i.e. all the ‘unknown’ Bessel beams have been correctly identified.

#### Modal characterization of Laguerre-Gaussian beam superposition.

In quantum optics, entanglement requires an analysis of superpositions of states. Such superpositions may also occur in the classical domain, for example when considering light fields with fractional azimuthal index<sup>30</sup>. It is therefore interesting to extend our approach to the more general case of a superposition of multiple Laguerre-Gaussian (LG) beams having different relative amplitudes and phases<sup>31</sup>. To that end, we trained the PCA eigenface algorithm on a set of 900 random complex superpositions (keeping the total intensity constant) of four LG beams ( $l = [0, 1]$  and  $p = [0, 1]$ ). A startling observation is that 97% of the whole training-set’s variability can be accounted for only the first nine principal components (Figure 6). Indeed, the superposition is described by four complex numbers leading to four real amplitudes and three relative phases. The non-linear relationship between these degrees of freedom and the far-field

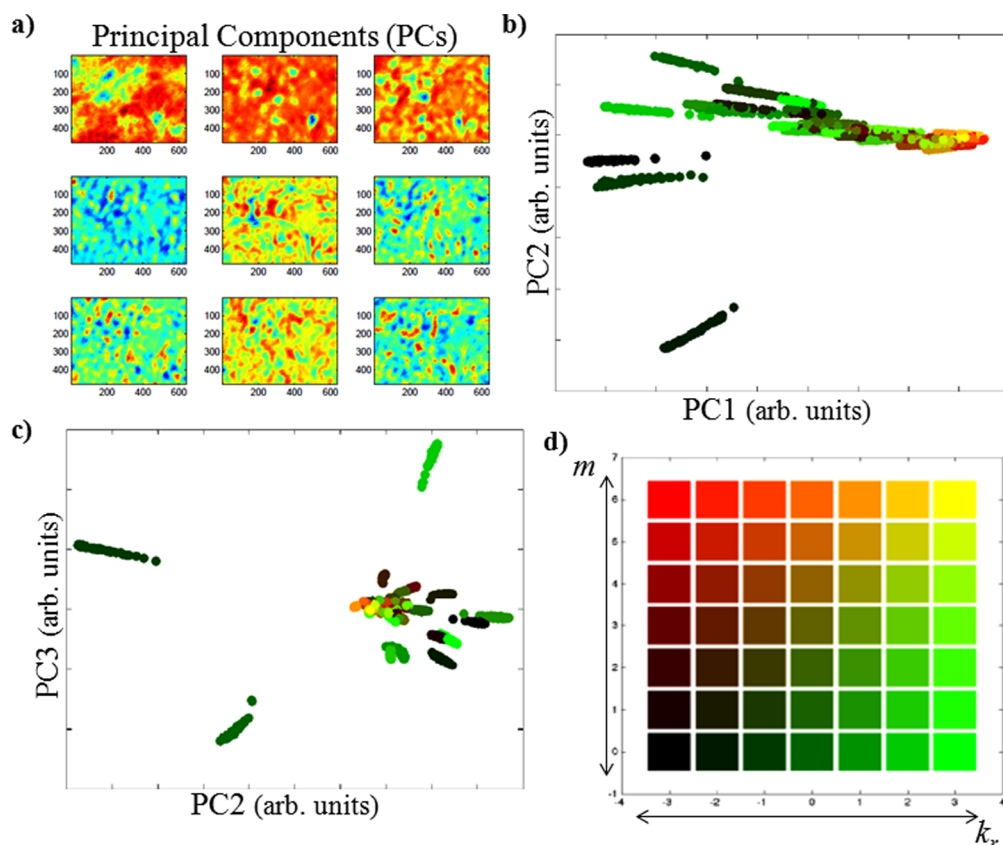


**Figure 5** | Modal characterization of the diffracted Bessel beams from a random aperture. (a) The first 9 principal components of the Bessel beam modes and their (b) first two principal components analysis, (c) second and third principal components analysis and (d) color coded for the azimuthal index  $m$  and the radial index  $k_r$ , of the Bessel beams considered.

diffraction pattern leads to the nine linear degrees of freedom observed experimentally (Figure 6a) and numerically (Figure 6c). Further, the projection onto these first principal components forms a dense cloud showing a non-normal distribution due to the constant intensity constraint (Figure 6b). Finally, we can identify the amplitude distribution of an unknown beam by using nearest neighbor classification. Experimentally, the best results were achieved when averaging over the six closest neighbors (see error histogram Figure 6d). The relative phase between the constituent beams can be retrieved by using an optical eigenmode<sup>32,33</sup> decomposition together with a Gerchberg-Saxton (GS) algorithm<sup>34</sup> (for more details see Supplementary information S3 and S5). The knowledge of these amplitudes and phases of the individual components makes their representation on a higher-order Poincaré sphere possible<sup>35</sup>.

## Discussion

This paper presents a powerful method by which the mode indices of both Hermite-Gaussian and Bessel beams can be determined. In addition to standard methods used to characterize higher-order beam modes, we have shown how the PCA algorithm can be used to characterize diffracted light modes. Our detection method is very simple to implement and uses a straightforward optical system (e.g. ground glass). It is based on the measurement of correlations between the probed far-field diffraction patterns and the ‘training set’ of preliminary recorded far-field diffraction patterns of the considered Hermite-Gaussian and Bessel beams. The Principal Component Analysis (PCA) algorithm calculates a projection of the ‘unknown’ beam onto the term of the mode composition. The experimental data show that the methodology preserves a high detectability in case of strong beam distortions (e.g. those caused

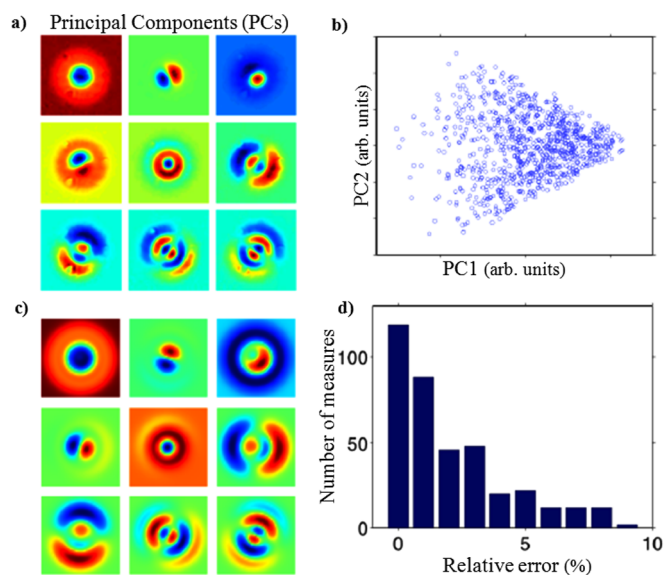


**Figure 6** | Modal characterization of the LG beam superposition. The first (a) experimental and (c) theoretical principal components deduced from 900 random LG beam superposition ( $l = [0, 1]$  and  $p = [0, 1]$ ), (b) first two principal component projections (experimental), (d) experimentally measured individual beam detection errors for a different set of 100 random superpositions. The intensity error is defined as  $(c_i - m_i)^2$  where  $c_i$  and  $m_i$  are the, encoded and respectively measured, real amplitude superposition coefficients.

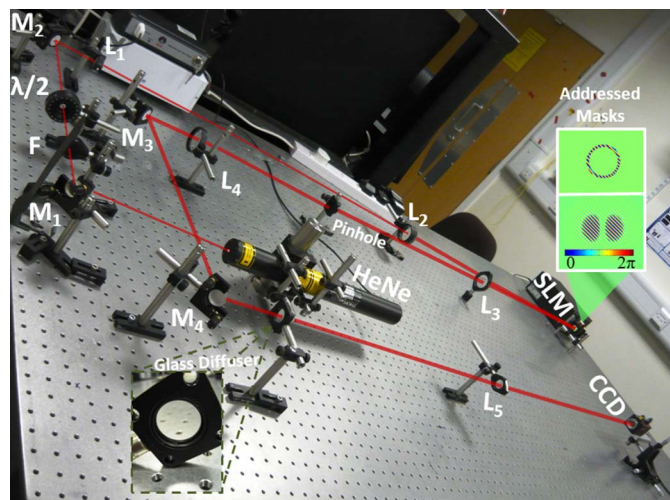


**Figure 7** | The experimental arrangement for the observation of the far-field diffraction patterns of Bessel beams, higher order Gaussian beams and their superposition from a glass diffuser. L = lens, SLM = spatial light modulator, M = mirror, CCD = charge couple device camera, F = ND filter. Focal lengths of lenses:  $f_1 = 150$  mm,  $f_2 = 1000$  mm,  $f_3 = 680$  mm,  $f_4 = 400$  mm, and  $f_5 = 800$  mm.

by a random aperture), provided that the ‘training set’ members undergo the same distortions. Thus, it is tolerant to misalignment, beam fluctuations, rotation, focusing and defocusing provided it has been ‘trained’ for these fluctuations. Furthermore, the used mask does not need any clever design or complicated mathematical framework. The shape of the diffracting mask used to measure the mode indices is in fact of little importance. The crucial step is ‘training’ any diffracting optical system and the ability to access a sufficiently large and relevant number of optical degrees of freedom<sup>29</sup>. This allows the transformation of the observed far-field diffraction pattern into uncorrelated variables (principal components) that can be mapped onto transversal mode profile index.

Our PCA detection method can be generalized to other orthogonal mode families, which will be useful for many applications relating the optical technologies, such as the modal decomposition for optical fibers, laser resonators and information processing. Our method is generic and may be extended to superpositions of different families of light fields. Here, the amplitudes of the different LG components in a limited superposition of LG beams were measured. In future work, we will test the applicability of the method to superposition of larger number of modes and study its limitations for general beam characterization.

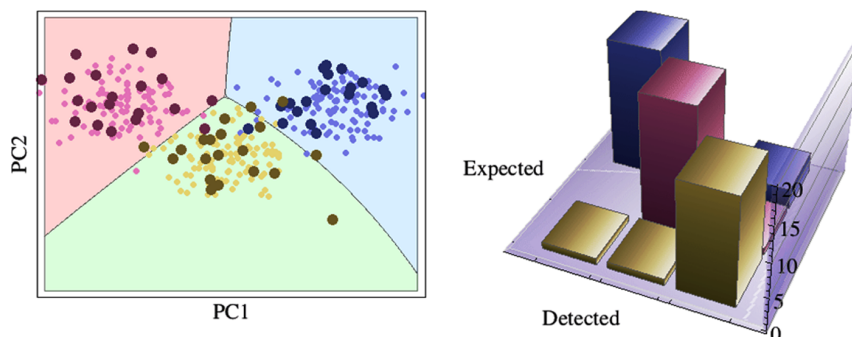


**Figure 8** | The PCA detection method. (See Supplementary video file S4) the video includes an animation in which the PCA algorithm is presented. To aid viewing the animation pauses after ‘training’ (cluster identification) and the classification of the ‘unknown’ data, so that the reader can view the construction of the 3D chart of the confusion matrix which depicts the efficiency of this method.

## Methods

The Hermite-Gaussian (HG) modes are described in part by the product of two-independent Hermite polynomials, for the field distribution in the  $x$  and  $y$  directions, respectively<sup>19</sup>. The values of  $m$  and  $n$  correspond to the number of nodes in the electromagnetic field. For example, the  $HG_{3,1}$  mode has three field nodes in the  $x$  and one in the  $y$  direction. The electric field,  $E(x, y, z)$ , transverse to the direction of propagation for the HG modes is given by:

$$E_{mn}(x, y, z) = E_0 \frac{w_0}{w(z)} \cdot H_m \left( \sqrt{2} \frac{x}{w(z)} \right) \exp \left( -\frac{x^2}{w(z)^2} \right) \cdot H_n \left( \sqrt{2} \frac{y}{w(z)} \right) \exp \left( -\frac{y^2}{w(z)^2} \right) \cdot \exp \left( -i \left[ kz - (1 + n + m) \arctan \frac{z}{z_R} + \frac{k(x^2 + y^2)}{2R(z)} \right] \right). \quad (1)$$

where the  $E_0$  is the field amplitude,  $R(z)$  is the radius of curvature,  $k$  is the wave-number of the electromagnetic wave, while  $x, y, z$  are the transverse positions within the beam and  $w(z)$  is the beam radius at which the Gaussian term falls to  $1/e$  of its axis value. In the above expression the Hermite-Gaussian beam functions alternate between even and odd symmetry with altering the  $m$  value. The  $m^{\text{th}}$ -order function has  $m$  nulls and  $m+1$  peaks. Most lasers preferentially oscillate in modes of rectangular rather than cylindrical symmetry, thus HG modes are very commonly used.

The electric field,  $E(r, \varphi, z)$ , of the Bessel beam is given by:

$$E(r, \varphi, z) = E_0 \cdot \exp(ik_z z) \cdot J_m(k_r r) \cdot \exp(\pm im\varphi) \quad (2)$$

where the  $E_0$  is the field amplitude,  $k_r$  and  $k_z$  are the radial and longitudinal components of the free-space wavevector, such that  $k = \sqrt{k_r^2 + k_z^2} = 2\pi/\lambda$ ,  $J_m$  is the Bessel function of the  $m^{\text{th}}$ -order and  $r, \varphi$  and  $z$  are the radial, azimuthal and longitudinal cylindrical coordinates respectively. The zero order Bessel beam has a transverse intensity profile with a central maximum spot surrounded by concentric rings. Whereas for all the higher-order Bessel beams, integer  $m \neq 0$ , the phase singularity of charge  $m$  on the beam axis results in a transverse intensity profile of concentric rings but with a phase singularity on the beam axis. This results in a ‘non-diffracting’ dark, rather than bright, core whose radius increases with the azimuthal index  $m$ . Due to their intensity profile and their reconstructed properties, these beams can find many applications in various fields<sup>36,37</sup>.

Nowadays both light fields, considered here, can be holographically generated using a computer controlled device, such as a spatial light modulator (SLM)<sup>38</sup>. The holograms were calculated according to the Equations (1) and (2) respectively; additionally the required phase distribution was imprinted onto the incident Gaussian beam which was illuminating the SLM. The optical Fourier transform of a HG function is always another HG function of the same order. In this study, the forty-nine lowest-order HG modes were created and analyzed.

For the Bessel beams study also far-field diffraction patterns of forty-nine different Bessel beam modes from a random aperture were respectively determined. Since, one way of interpreting the Bessel beam is to consider a set of plane waves propagating on a cone. This decomposition of the Bessel beam into plane waves manifests itself in the angular spectrum of the beam, which is an annulus in  $k$ -space. Here, annuli were displayed on the SLM which when Fourier transformed created the different Bessel beams considered. A wavefront correction to all beams was applied using the optical eigenmode (OEi) decomposition technique<sup>32,33</sup>.

The experimental set-up used is shown in Figure 7 and is similar to that used previously<sup>15</sup>. A laser beam (He-Ne,  $\lambda = 633$  nm,  $P_{\text{max}} = 5$  mW) with an output Gaussian profile of beam waist  $w = 5$  mm, was expanded using a dual lens telescope ( $L_1$  and  $L_2$ ). A half-wavelength ( $\lambda/2$ ) plate was used in order to rotate the polarization of the incoming beam to the optimum angle for the SLM (Holoeye, LC-R 2500) and maximize the power diffracted into the first order. The polarization state was verified by the use of a polarized beam-splitter after the half-wavelength ( $\lambda/2$ ) plate. The holograms used to generate the Hermite-Gaussian and Bessel beams were displayed on the SLM. A lens ( $L_3$ ) and a pinhole were introduced to the beam path to allow for



spatial filtration to block all the unwanted diffraction orders. Then, a lens ( $L_4$ ) was used to image the different laser beam modes on the random aperture, which in our case was a glass diffuser (Edmund Optics,  $0.5^\circ$  diffusing angle). We ensured that the angle of incidence of the incoming beam was as small as possible (preferably  $< 10^\circ$ ) in order to get the maximum diffraction efficiency. Finally, lens  $L_5$  served to create the far-field diffraction patterns in its back focal plane where a CCD camera (pike, Allied Vision Technologies) was used, in order to record and save the patterns onto the hard-drive of a computer.

**Detection through ‘eigenface’ classification.** Principal component analysis (PCA) algorithm refers to an algorithm that uses an orthogonal transformation in order to convert a set of observed data of possibly correlated variables into a set of linearly independent and uncorrelated variables called principal components (PCs) or ‘eigenfaces’<sup>39</sup>. The main goal of the PCA algorithm is to reduce the dimensionality of the data set. The number of the PCs is less than or equal to the number of the original observed data. This orthogonal transformation is defined in such a way that the first principal component (PC1) has the largest possible variance within the set of measures and each subsequent component reflects the next highest variance possible under the constraint that it be orthogonal to the components considered. The resultant PCs or ‘eigenfaces’ are ordered such that few of them can be used in order to account for most of the variation in all the original data set. Thus, a simpler basis can be provided for the further multivariate analysis of the data<sup>40</sup>. Whilst PCA has been established for over one hundred years (a technique dated back to 1901)<sup>39</sup> and widely applied in various areas, e.g. face recognition<sup>41</sup> and cancer detection<sup>42</sup>, this method has been recently considered or used in the case of diffraction theory and the analysis of the transverse state of a light field<sup>15</sup>.

The first step of applying the PCA algorithm to our study corresponds to creating a database of all possible Hermite-Gaussian or Bessel beams that we wish to detect. After subtraction of the common mean intensity, the covariance matrix of the recorded intensity patterns is calculated. Then, the resultant eigenvector with the largest eigenvalue is termed the first ‘eigenface’ which corresponds to the largest variability of the Hermite-Gaussian or Bessel beam modes ‘training set’. In the same way, the second ‘eigenface’ corresponds to the second largest variability of the covariance matrix and so on. Projecting the measured beams onto these ‘eigenfaces’, we determine the first and subsequent principal components (PCs) representation of the measure. The Hermite-Gaussian or Bessel beams with the same (mode indices) variables form very tight clusters (Figure 8), due to the readout noise and small vibrations of the optical system. Finally, a classification algorithm of the nearest neighbor is applied in order to classify the ‘unknown’ data<sup>24</sup>. However, other methods such as the Mahalanobis distance can be also applied<sup>43</sup>. Figure 8, shows the 3D chart of the confusion matrix, displaying the efficiency of this method i.e. whether all the ‘unknown’ beam modes have been correctly identified as the expected beam modes. The ideal confusion matrix is the identity matrix.

- Zurek, W. H. Reversibility and Stability of Information Processing Systems. *Phys. Rev. Lett.* **53**, 391–394 (1984).
- Siegman, A. E. Hermite-gaussian functions of complex argument as optical-beam eigenfunctions. *J. Opt. Soc. Am.* **63**, 1093–1094 (1973).
- Shapira, O., Abouraddy, A. F., Joannopoulos, J. D. & Fink, Y. Complete Modal Decomposition for Optical Waveguides. *Phys. Rev. Lett.* **94**, 143902 (2005).
- Schimpf, D. N. & Ramachandran, S. Polarization-resolved imaging of an ensemble of waveguide modes. *Opt. Lett.* **37**, 3069–3071 (2012).
- Beom Soo Soh, D. *et al.* Modal power decomposition of beam intensity profiles into linearly polarized modes of multimode optical fibers. *J. Opt. Soc. Am. A* **21**, 1241–1250 (2004).
- Bekshaev, A. Y., Soskin, M. S. & Vasnietsov, M. V. Optical vortex symmetry breakdown and decomposition of the orbital angular momentum of light beams. *J. Opt. Soc. Am. A* **20**, 1635–1643 (2003).
- Molina-Terriza, G., Vaziri, A., Řeháček, J., Hradil, Z. & Zeilinger, A. Triggered Qutrits for Quantum Communication Protocols. *Phys. Rev. Lett.* **92**, 167903 (2004).
- Berkhout, G. C. G. & Beijersbergen, M. W. Method for Probing the Orbital Angular Momentum of Optical Vortices in Electromagnetic Waves from Astronomical Objects. *Phys. Rev. Lett.* **101**, 100801 (2008).
- Mourka, A., Baumgartl, J., Shanor, C., Dholakia, K. & Wright, E. M. Visualization of the birth of an optical vortex using diffraction from a triangular aperture. *Opt. Express* **19**, 5760–5771 (2011).
- Hickmann, J. M., Fonseca, E. J. S., Soares, W. C. & Chávez-Cerda, S. Unveiling a Truncated Optical Lattice Associated with a Triangular Aperture Using Light’s Orbital Angular Momentum. *Phys. Rev. Lett.* **105**, 053904 (2010).
- Ferreira, Q. S., Jesus-Silva, A. J., Fonseca, E. J. S. & Hickmann, J. M. Fraunhofer diffraction of light with orbital angular momentum by a slit. *Opt. Lett.* **36**, 3106–3108 (2011).
- Sztul, H. I. & Alfano, R. R. Double-slit interference with Laguerre-Gaussian beams. *Opt. Lett.* **31**, 999–1001 (2006).
- Berkhout, G. C. G., Lavery, M. P. J., Padgett, M. J. & Beijersbergen, M. W. Measuring orbital angular momentum superpositions of light by mode transformation. *Opt. Lett.* **36**, 1863–1865 (2011).
- Berkhout, G. C. G., Lavery, M. P. J., Courial, J., Beijersbergen, M. W. & Padgett, M. J. Efficient Sorting of Orbital Angular Momentum States of Light. *Phys. Rev. Lett.* **105**, 153601 (2010).

- Mazilu, M., Mourka, A., Vettenburg, T., Wright, E. M. & Dholakia, K. Simultaneous determination of the constituent azimuthal and radial mode indices for light fields possessing orbital angular momentum. *Appl. Phys. Lett.* **100**, 231115 (2012).
- Abouraddy, A. F., Yarnall, T. M. & Saleh, B. E. A. Angular and radial mode analyzer for optical beams. *Opt. Lett.* **36**, 4683–4685 (2011).
- Kogelnik, H. & Li, T. Laser Beams and Resonators. *Appl. Opt.* **5**, 1550–1567 (1966).
- Novotny, L., Sánchez, E. J. & Sunney Xie, X. Near-field optical imaging using metal tips illuminated by higher-order Hermite-Gaussian beams. *Ultramicroscopy* **71**, 21–29 (1998).
- Siegman, A. E. Lasers. *Universe Science Books*, 642–652 (1986).
- Garces-Chavez, V., McGloin, D., Melville, H., Sibbett, W. & Dholakia, K. Simultaneous micromanipulation in multiple planes using a self-reconstructing light beam. *Nature* **419**, 145–147 (2002).
- Tsamppoula, X. *et al.* Femtosecond cellular transfection using a nondiffracting light beam. *Appl. Phys. Lett.* **91**, 053902 (2007).
- Fahrbach, F. O., Simon, P. & Rohrbach, A. Microscopy with self-reconstructing beams. *Nat. Photon.* **4**, 780–785 (2010).
- Bennett, C. H. & DiVincenzo, D. P. Quantum information and computation. *Nature* **404**, 247–255 (2000).
- Cover, T. & Hart, P. Nearest neighbor pattern classification. *IEEE Trans. Inf. Theory* **13**, 21–27 (1967).
- Beijersbergen, M. W., Allen, L., van der Veen, H. E. L. O. & Woerdman, J. P. Astigmatic laser mode converters and transfer of orbital angular momentum. *Opt. Commun.* **96**, 123–132 (1993).
- Padgett, M., Arlt, J., Simpson, N. & Allen, L. An experiment to observe the intensity and phase structure of Laguerre-Gaussian laser modes. *Am. J. Phys.* **64**, 77–82 (1996).
- Abramochkin, E. & Volostnikov, V. Beam transformations and nontransformed beams. *Opt. Commun.* **83**, 123–135 (1991).
- Habraken, S. J. M. & Nienhuis, G. Modes of a rotating astigmatic optical cavity. *Phys. Rev. A* **77**, 053803 (2008).
- Piestun, R. & Miller, D. A. B. Electromagnetic degrees of freedom of an optical system. *J. Opt. Soc. Am. A* **17**, 892–902 (2000).
- Götte, J. B. *et al.* Light beams with fractional orbital angular momentum and their vortex structure. *Opt. Express* **16**, 993–1006 (2008).
- Vaziri, A., Weihs, G. & Zeilinger, A. Superpositions of the orbital angular momentum for applications in quantum experiments. *J. Opt. B: Quantum Semiclass. Opt.* **4**, S47–S51 (2002).
- De Luca, A. C., Kosmeier, S., Dholakia, K. & Mazilu, M. Optical eigenmode imaging. *Phys. Rev. A* **84**, 021803 (2011).
- Mazilu, M., Baumgartl, J., Kosmeier, S. & Dholakia, K. Optical Eigenmodes; exploiting the quadratic nature of the energy flux and of scattering interactions. *Opt. Express* **19**, 933–945 (2011).
- Saxton, R. G. A. W. A practical algorithm for the determination of the phase from image and diffraction plane pictures. *Optik* **35**, 237–246 (1972).
- Milione, G., Sztul, H. I., Nolan, D. A. & Alfano, R. R. Higher-Order Poincaré Sphere, Stokes Parameters, and the Angular Momentum of Light. *Phys. Rev. Lett.* **107**, 053601 (2011).
- McGloin, D. & Dholakia, K. Bessel beams: diffraction in a new light. *Contem. Phys.* **46**, 15–28 (2005).
- Mazilu, M., Stevenson, D. J., Gunn-Moore, F. & Dholakia, K. Light beats the spread: “non-diffracting” beams. *Laser Photonics Rev.* **4**, 529–547 (2010).
- Vasara, A., Turunen, J. & Friberg, A. T. Realization of general nondiffracting beams with computer-generated holograms. *J. Opt. Soc. Am. A* **6**, 1748–1754 (1989).
- Pearson, K. LIII. On lines and planes of closest fit to systems of points in space. *Philos. Mag.* **2**, 559–572 (1901).
- Everitt, B. & Hothorn, T. In *An Introduction to Applied Multivariate Analysis with R*, Springer New York, Ch. 3, 61–103 (2011).
- Peter, N. B. Eigenfaces vs. Fisherfaces: Recognition Using Class Specific Linear Projection. *IEEE T. Pattern Anal.* **19**, 711–720 (1997).
- van’t Veer, L. J. *et al.* Gene expression profiling predicts clinical outcome of breast cancer. *Nature* **415**, 530–536 (2002).
- Draper, B. A., Baek, K., Bartlett, M. S. & Beveridge, J. R. Recognizing faces with PCA and ICA. *Comput. Vis. Image Und.* **91**, 115–137 (2003).

## Acknowledgements

We thank the UK Engineering and Physical Sciences Research Council for funding. Kishan Dholakia is a Royal Society-Wolfson Merit Award Holder.

## Author contributions

All authors developed and planned the project. A.M. performed the experimental work; M.M. analyzed the data and all authors wrote, reviewed and approved the manuscript.

## Additional information

Supplementary information accompanies this paper at <http://www.nature.com/scientificreports>



**Competing financial interests:** The authors declare no competing financial interests.

**License:** This work is licensed under a Creative Commons Attribution-NonCommercial-NoDerivs 3.0 Unported License. To view a copy of this license, visit <http://creativecommons.org/licenses/by-nc-nd/3.0/>

**How to cite this article:** Mourka, A., Mazilu, M., Wright, E.M. & Dholakia, K. Modal Characterization using Principal Component Analysis: application to Bessel, higher-order Gaussian beams and their superposition. *Sci. Rep.* 3, 1422; DOI:10.1038/srep01422 (2013).